SCIENCE CHINA Materials LETTER

mater.scichina.com link.springer.com

Published online 3 December 2020 | https://doi.org/10.1007/s40843-020-1503-7
Sci China Mater 2021, 64(3): 783–788

A large format aqueous rechargeable $LiMn_2O_4$/Zn battery with high energy density and long cycle life

Zhiguo Hou[1*], Xueqian Zhang[1], Mengfei Dong[1], Yali Xiong[1], Zixiang Zhang[1], Huaisheng Ao[2], Mengke Liu[2], Yongchun Zhu[2] and Yitai Qian[2*]

Zinc (Zn) has been regarded as the most promising anode material for aqueous rechargeable batteries because of its high theoretical capacity (820 mA h g^{-1}), moderate electrochemical potential (−0.762 V *vs.* the standard hydrogen electrode (SHE)), low cost and environmental friendliness [1–3]. For cathodes coupled with Zn anode, there are two types of materials mainly reported: nickel hydroxide which operates *via* conversion, not intercalation, has been reported to be remarkably effective in sustaining long-life cycling in Zn batteries [4]; vanadium oxide [5–11] and prussian blue analogues [12–14] have been explored for reversible Zn^{2+} intercalation. These cathodes display excellent rate performance, high cyclic stability and voltage, respectively. Moreover, manganese dioxide (MnO_2) in various phases, such as α-MnO_2 [15–19], β-MnO_2 [20], γ-MnO_2 [21], δ-MnO_2 [22], and other types, have been reported because of its low-cost, non-toxicity and relatively high theoretical capacity (308 mA h g^{-1}). However, MnO_2 with different structures has been demonstrated to have different reaction mechanisms. Zn^{2+} intercalation in the MnO_2 framework was reported as the main charge storage mechanism for MnO_2 with layered structure, such as tunnel-type $Zn_xMn_2O_4$ [23], layered birnessite [24], layered Zn-buserite, and/or their complex composite. Reversible conversion reactions were commonly reported for tunnel type MnO_2. Recently, Chen's group [25] reported Zn^{2+} intercalation in the spinel $ZnMn_2O_4$.

It is important to point out that $LiMn_2O_4$ (LMO) is the most promising cathode material for fast lithium ion migration kinetics and high potential [26,27]. It has been reported that using LMO in aqueous electrolytes with Li-based salts, the battery shows little capacity attenuation after tens of thousands of full cycles [28], which greatly decreases the processing/synthesis cost of this material, suggesting it is a good candidate for stationary energy storage application. However, most of the previous work achieved high electrochemical performance based on button battery by using less than 10 mg active materials with the low areal capacity and limited system energy density, which suggests that large cells need to further develop for practical application [29–32].

To prove the feasibility of aqueous zinc ion batterys (AZIBs) for practical application, Parker *et al.* [33] constructed Ni-three-dimensional (3D) Zn single cells (such as pouch cells *vs.* larger coin cells). Chen and co-workers [34] reported a flexible Zn/NaV_3O_8·1.5H_2O (NVO) pouch battery that was assembled by sandwiching quasi-solid-state gelation/$ZnSO_4$ electrolyte between the NVO positive electrode and Zn foil. Zhou *et al.* [35] demonstrated a commercial-grade 3.5 A h Ni-Zn pouch battery, which presents a record high gravimetrical energy density of 165 W h kg^{-1} and volumetrical energy density of 506 W h L^{-1} based on the whole battery.

In this study, we reported a commercial-grade rechargeable AZIB based on LMO cathode, Zn anode and 1 mol L^{-1} Li_2SO_4/$ZnSO_4$ electrolyte with 8 mol L^{-1} urea additive. The battery delivered stability over 500 cycles with energy density of 80 W h kg^{-1} and low cost of 50 $ per kW h. A novel corrosion-resistant cathode current collector composed of graphite-coated nylon (GCN) membrane was developed with low cost and lightweight, which contributed to an important step for AZIBs, thereby increasing the energy density. To date, the dissolution of manganese in aqueous electrolyte and oxygen evolution reaction on cathode still need to be optimized. In this system, the electrochemical reaction of urea produced solid product insoluble in aqueous media, which

[1] School of Chemical and Environmental Engineering, Jiangsu University of Technology, Changzhou 213001, China
[2] School of Chemistry and Materials, University of Science and Technology of China, Hefei 230026, China
* Corresponding authors (emails: houzhigu@mail.ustc.edu.cn (Hou Z); ytqian@ustc.edu.cn (Qian Y))

deposited on the surfaces of electrodes, forming solid electrolyte interface (SEI), thereby suppressing the Mn^{2+} dissolution, and helping to maintain the cathode structure integrity. Furthermore, zinc metal anode undergoes two typically undesirable regimes, such as the formation of dendrites that leads to electrical-short-circuits and the precipitation of ZnO that can irreversibly passivate Zn surface. Here, the Zn anode exhibits excellent reversibility because the urea is a strong-field ligand towards to Zn^{2+}, which takes part in the Zn^{2+} solvation sheath, significantly suppressing the presence of $(Zn(H_2O)_6)^{2+}$. As a result, the full battery exhibits long cycle life. Our results will be of benefit in the development of safe, low-cost and high-performance Zn battery for applications in practical energy storage, low-speed electric bicycle and so on.

The as-prepared GCN collector is smooth and the graphite sheets are contacted with each other, which guarantees the high electronic conductivity (as shown in Fig. S1). The GCN membrane current collector is corrosion-resistant and light-weight, compared with traditional stainless steel (SS) current collector. As shown in Fig. S2, the linear scan voltammetry results for different current collectors in 1 mol L^{-1} Li_2SO_4 + 1 mol L^{-1} $ZnSO_4$ electrolyte (named as 1-1 electrolyte) at a scan rate of 0.5 mV s^{-1} show that the Pt current collector is the most stable without oxidation. The SS suffers from pitting corrosion at 3.9 V. Since the working potential of LMO is between 3.8 and 4.3 V, the SS collector is thermodynamically unstable in aqueous electrolyte. The linear scan voltammetry result for the as-prepared GCN current collector in 1-1 electrolyte shows that there is no obvious oxidation, suggesting its good corrosion resistance. The GCN was used as cathode current collector, and the Cu foil was used as anode current collector, because the hydrogen evolution potential of Cu foil is more negative than that of GCN (as shown in Fig. S3).

The Zn anode in aqueous electrolytes usually suffers from irreversibility issues caused by the low Coulombic efficiency (CE) of its plating/stripping and irreversible by-products, such as Zn hydroxides or zincates. It has been reported that the strong interaction between Zn^{2+} and water molecules results in a high energy barrier for the solvated Zn^{2+} to desolvate and deposit, whereas the generation of OH^- *via* water decomposition often drives the formation of $Zn(OH)_2$, which further converts into electrochemically inactive ZnO [30]. To weaken the strong interaction between Zn^{2+} and water molecules, urea was added into the 1-1 electrolyte. The interaction among Zn^{2+}, urea and water was qualitatively analyzed using nuclear magnetic resonance (NMR) spectroscopy. The ^1H NMR spectra of different electrolytes were tested (as shown in Fig. S4). The two sets of oxygen nuclei were assigned to water (~4.8 ppm) and urea (~5.7 ppm), respectively. Since a downfield signal (higher chemical shift) indicates a weaker electronic density around hydrogen, this observation corroborates a strong Zn^{2+}-water interaction. The ^1H signal from urea has a greatly higher chemical shift (downfield) for 1-1-8 electrolyte (6.3 ppm) compared with that of 1 mol L^{-1} urea added in 1-1 electrolyte (5.7 ppm). It suggests that the urea should crowd into the Zn^{2+} primary solvation shell structure in 1-1-8 electrolyte. Evidence also comes from the pH of different electrolytes. The pH of 1-1 electrolyte is 4.5 and the pH of 1-1-8 electrolyte is 6.9 (Fig. S5).

With a slower scaning rate of 0.05 mV s^{-1}, a tiny oxidation peak appeared at about 4.0 V in 1-1-8 electrolyte (Fig. S6a), which should be ascribed to the oxidation of urea:

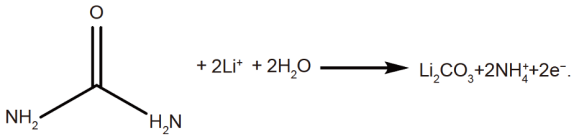

The oxidation of urea formed lithium salt Li_2CO_3, which deposited on the surface of the electrode, forming a solid state layer. Because of the oxidation of urea, it is possible to form SEI layer. To further confirm it, the C 1s X-ray photoelectron spectroscopy (XPS) measurements of Pt electrode after linear sweep voltammetry test were carried out. As shown in Fig. S6b, the XPS result of Pt electrode after linear sweep voltammetry in 1-1-8 solution confirms the presence of Li_2CO_3. Therefore, the urea can be oxidized to form Li_2CO_3, which is beneficial to forming SEI. The weakened Zn-water interaction essentially eliminated the hydrolysis effect. The CE of Zn plating/stripping in 1-1-8 electrolyte is about 99.5%, which is much higher than that in 1-1 electrolyte (as shown in Fig. S7). To obtain both long cycle life and high energy density, the mass ratio of cathode and anode was set to 0.4.

Large-format devices of sufficient energy density were implemented. The battery was assembled by a stack method. The electrolyte was 1-1-8 electrolyte. Fig. 1a shows the typical charge/discharge profiles of the large-format battery at a current of 1 A. The initial charge capacity is 11 A h and the initial discharge capacity is about 10 A h, exhibiting an initial CE of 91%. The energy density is 140 W h kg^{-1} based on the total mass of cathode and anode. The practical energy density is

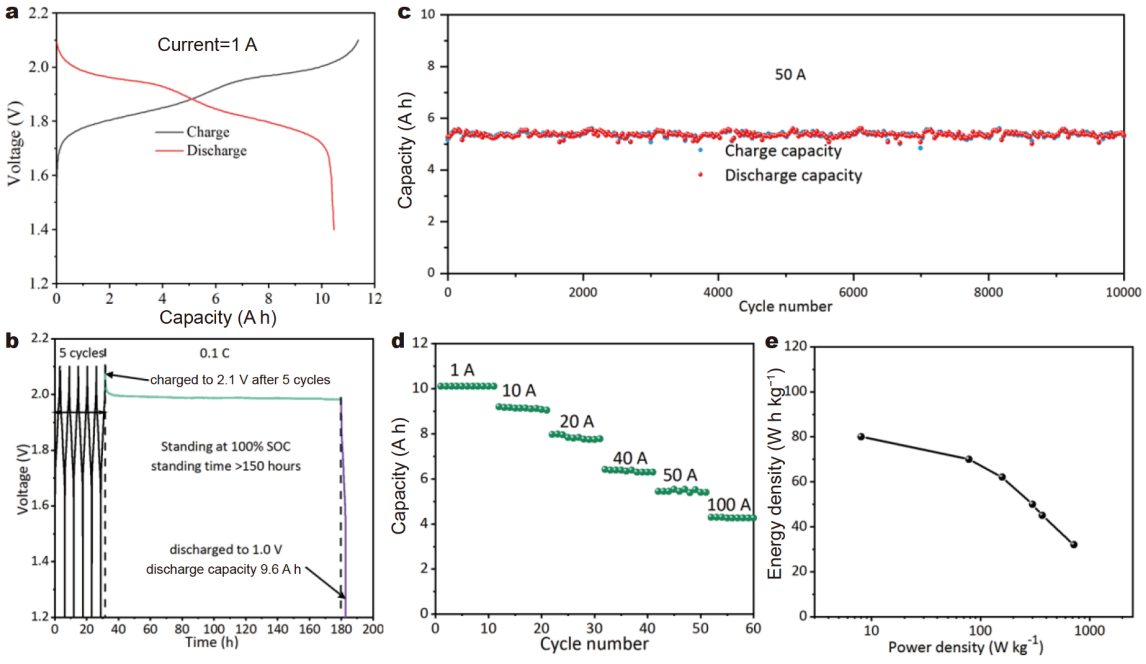

Figure 1 (a) The typical charge/discharge profiles of the large-format battery at a current of 1 A. (b) The self-discharge performance. (c) The cycle performance of battery at a charging/discharging current of 50 A. (d, e) The rate performance and Ragone plots of the battery.

80 W h kg^{-1} and the cost of the battery is about 50 $ per kW h (as shown in Table S1). Practical battery must possess the ability to hold charge over extended periods with little or no self-discharge at 100% state of charge (SOC). To examine the self-discharge characteristics of this battery, a battery was deep cycled 5 times, the cell was then left to stand at open circuit for 150 h, and then the cycling was resumed. As shown in Fig. 1b, after about 150 h resting at 100% SOC, the battery can deliver a discharge capacity of 9.6 A h. Only a slight capacity of 0.4 A h is lost, indicating an extremely slow rate of self-discharge. As shown in Fig. 1c, the battery exhibits as long as 10,000 cycles life at a charging/discharging current of 50 A. The battery also exhibits good rate capability. A specific discharge capacity of about 4.5 A h is achieved at a high current of 100 A (shown in Fig. 1d), which is about 45% of the capacity at 1 A. As shown in Fig. 1e, the specific energy of the battery still remains 32 W h kg^{-1} at a high power of 720 W kg^{-1}.

This battery displays excellent cycle stability with 90% capacity retention after 400 cycles. Moreover, the battery can function well at temperature as low as 0°C, showing a 70% discharge capacity retention relative to 25°C (as shown in Fig. S8). The viscosity is low (8 mPa s at 25°C), but the ionic conductivity is very high (15 mS cm^{-1} at 25°C) (as shown in Fig. S9). It should be ascribed to the high ion conductivity and low viscosity of 1-1-8 electrolyte. As reported previously, LMO suffers from a more severe capacity fading at elevated temperature [21]. The battery exhibits good cycle stability at a high temperature of 50°C. The large-format prismatic battery remains stable with capacity retention of about 85% after 400 cycles at a current of 10 A. The prototype battery (10 A h) is only 236 g, as illustrated in Fig. 2. The size of the battery is labeled in Fig. 2. The height, width and thickness are 0.09, 0.1 and 0.01 m. The volumetric energy density of the battery is about 200 W h L^{-1}.

The above results demonstrated that in 1-1-8 electrolyte the battery exhibited superior cycling performance and high CE at low rate of 0.1 C. It should be ascribed to the formation of SEI layer on the surface of cathode. To confirm that SEI layer has been formed, high resolution-transmission electron microscopy (HR-TEM) images and XPS results of LMO cathode after 10,000 cycles were collected as direct evidence. The surfaces of LMO were imaged after 10,000 cycles in 1-1-8 electrolyte (Fig. 3a). An extra layer of partially crystalline species with the thickness of about 15 nm was detected, on the surface of LMO (as shown in Fig. 3a and the inset). The interplanar space of this new layer is about 0.42 nm, which is almost identical to the crystalline Li_2CO_3 (0.418 nm (110)). XPS also detected additional C 1s signal at 290.5 eV and O 1s

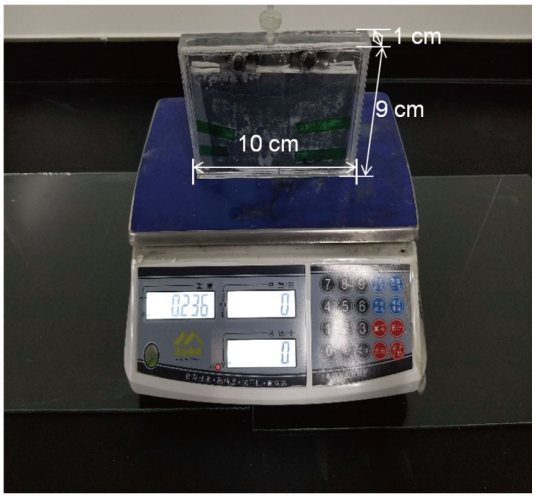

Figure 2 Schematic diagram of a prototype battery with a weight of 236 g (10 A h).

signal at 531.5 eV corresponding to Li_2CO_3 on the cycled LMO (Fig. 3b, c). The Zn 2p XPS result of LMO after discharged process shows no signal of Zn, which suggests that there should be no Zn intercalation/deintercalation into/from the LMO cathode (as shown in Fig. S10). Both TEM and XPS directly confirm the presence of an interphase that primarily consists of Li_2CO_3 on the surface of LMO cathode. The surfaces of LMO electrodes after cycling in 1-1 electrolyte for 100 cycles were also imaged as a reference. The TEM image shows that the smooth edges of pristine material became rough with small notches after 15 cycles in 1-1 electrolyte (Fig. S11). The TEM and XPS results show that the SEI layer is absent on the LMO surface. Evidence also comes from X-ray diffraction (XRD) and inductively coupled plasma-atomic emission spectroscopy (ICP-AES) tests. The XRD results of electrodes after 10,000 cycles show that the electrodes cycled in 1-1-8 electrolyte retain good crystallinity (Fig. S12). However, the diffraction peaks of LMO are weakened and there are emerged peaks of $Mn(OH)_2$ after 100 cycles in 1-1 electrolyte. In addition, Mn dissolution is more serious in 1-1 electrolyte after 100 cycles than that in 1-1-8 electrolyte after 10,000 cycles, as evidenced by the ICP-AES analysis (Table S2). Thus, it suggests that the SEI layer inhibits Mn dissolution, maintains LMO structural integrity, and hence improves the cycle performance of LMO.

The Zn anode was also examined in an effort to understand the high reversibility of the LMO/Zn cell chemistry. The reversibility and stability of Zn in different electrolytes were investigated using a Zn/Zn symmetric cell under galvanostatic condition, respectively. Fig. 4a displays the typical voltage profiles at a constant charge and discharge current density of 1 mA cm^{-2}. In the 1-1 electrolyte, there is a sudden increase in polarization after 30 h for only 15 cycles of Zn stripping and plating, which could be attributed to the formation of an insulating ZnO and $Zn(OH)_2$ powder layer on the anode surface (shown by the XRD pattern in Fig. S13) and a loose dendrite-like of Zn plate surface after cycling (shown in Fig. S14). In contrast, in 1-1-8 electrolyte, the Zn/Zn symmetric cell shows the excellent reversibility and stability of Zn stripping/plating. After 400 cycles (corresponding to 800 h), the charge and discharge potential keep almost unchanged. As shown in Fig. 4b, after more than 400 cycles, the Zn anode still exhibits a smooth, dense surface. It can be seen that the Zn deposits formed on the anode are well directed, showing an orientation relation with the (002) crystal face (as shown in inset of Fig. 4b). Evidence also comes from XRD data. Specifically, if Zn plates are assumed to orient parallel to the (001)-type reflections, XRD intensities of Zn (002) should be higher, relative to (*hk*0)-type reflections, e.g., Zn (100). This is in fact precisely by comparing the Zn (002) to Zn (100) peak intensity ratio for the Zn deposits. In the 1-1-8 electrolyte, the Zn (002)/Zn (100) ratios is 2.05, and it is 1.25 in 1-1 electrolyte (as shown in Fig. 4c and Fig. S13, respectively).

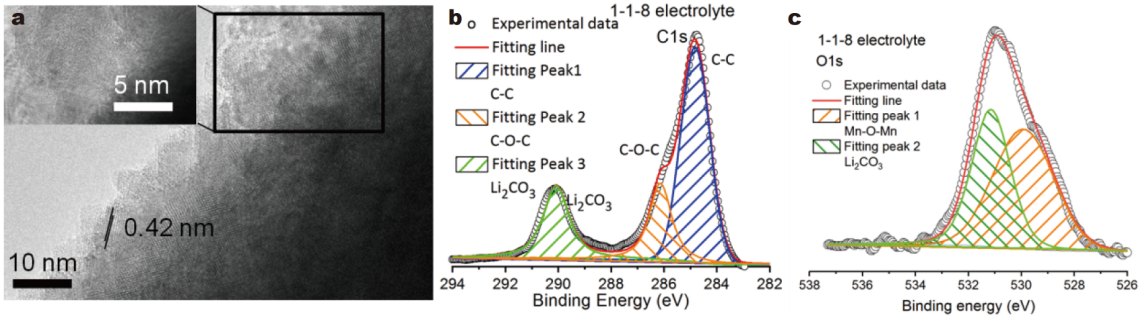

Figure 3 (a) HR-TEM image, (b) C 1s XPS results and (c) O 1s XPS profiles of LMO cathode after 10,000 cycles in 1-1-8 electrolyte.

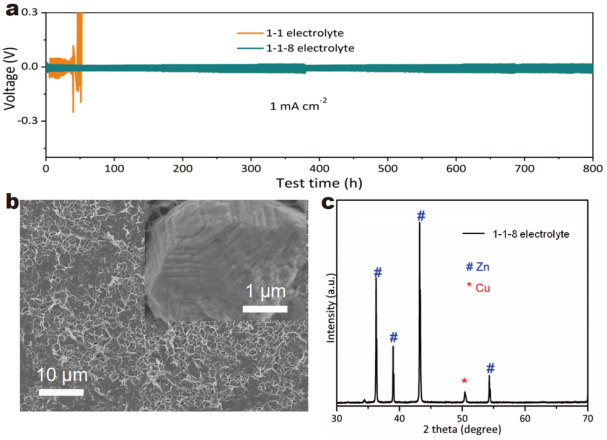

Figure 4 (a) Voltage responses of Zn/Zn symmetric cells in 1-1-8 electrolyte and 1-1 electrolyte at 1 mA cm^{-2} (1 mA h cm^{-2} for each half cycle) for 400 cycles, respectively. (b, c) Scanning electron microscopy (SEM) image and XRD pattern of Zn anode after 400 stripping/plating cycles in 1-1-8 electrolyte.

The ordered growth of Zn deposition effectively avoids the formation of Zn dendrite. In addition, the passivation of Zn is also inhibited as shown in Fig. 4c and Fig. S13.

In summary, a scalable cost-effective preparation of practical LMO/Zn batteries was developed for the first time and the elaborate commercial-grade 10 A h LMO/Zn pouch battery possesses unprecedented gravimetrical energy density of 80 W h kg^{-1} (weight, 236 g/10 A h) and volumetrical energy density of 200 W h L^{-1}, which is safe and affordable (50 $ per kW h). A best practice for systematical measuring of the aqueous batteries and electrode materials in a more practical metric were demonstrated. The single battery delivers 90% capacity retention at 25°C and 85% capacity retention at high temperature of 50°C after 400 cycles at 10 A. This study is a fillip for the development of high energy and power density aqueous batteries, and will be of benefit for next-generation reliable, affordable and scalable energy storage.

Received 1 July 2020; accepted 24 August 2020; published online 3 December 2020

1 Tian Y, An Y, Wei C, *et al.* Flexible and free-standing $Ti_3C_2T_x$ MXene@Zn paper for dendrite-free aqueous zinc metal batteries and nonaqueous lithium metal batteries. ACS Nano, 2019, 13: 11676–11685

2 Tang B, Shan L, Liang S, *et al.* Issues and opportunities facing aqueous zinc-ion batteries. Energy Environ Sci, 2019, 12: 3288–3304

3 Ma L, Schroeder MA, Pollard TP, *et al.* Critical factors dictating reversibility of the zinc metal anode. Energy Environ Mater, 2020, doi: 10.1002/eem2.12077

4 Li JL, Aslam MK, Chen CG. One-pot hydrothermal synthesis of porous α-$Ni(OH)_2$/C composites and its application in Ni/Zn alkaline rechargeable battery. J Electrochem Soc, 2018, 165: A910–A917

5 Chen L, Ruan Y, Zhang G, *et al.* Ultrastable and high-performance Zn/VO_2 battery based on a reversible single-phase reaction. Chem Mater, 2019, 31: 699–706

6 Dai X, Wan F, Zhang L, *et al.* Freestanding graphene/VO_2 composite films for highly stable aqueous Zn-ion batteries with superior rate performance. Energy Storage Mater, 2019, 17: 143–150

7 Ding J, Du Z, Gu L, *et al.* Ultrafast Zn^{2+} intercalation and deintercalation in vanadium dioxide. Adv Mater, 2018, 30: 1800762

8 Wang X, Xi B, Feng Z, *et al.* Layered $(NH_4)_2V_6O_{16}·1.5H_2O$ nanobelts as a high-performance cathode for aqueous zinc-ion batteries. J Mater Chem A, 2019, 7: 19130–19139

9 Wang P, Shi X, Wu Z, *et al.* Layered hydrated vanadium oxide as highly reversible intercalation cathode for aqueous Zn-ion batteries. Carbon Energy, 2020, 2: 294–301

10 Kundu D, Adams BD, Duffort V, *et al.* A high-capacity and long-life aqueous rechargeable zinc battery using a metal oxide intercalation cathode. Nat Energy, 2016, 1: 16119

11 Wang L, Huang KW, Chen J, *et al.* Ultralong cycle stability of aqueous zinc-ion batteries with zinc vanadium oxide cathodes. Sci Adv, 2019, 5: eaax4279

12 Wang LP, Wang PF, Wang TS, *et al.* Prussian blue nanocubes as cathode materials for aqueous Na-Zn hybrid batteries. J Power Sources, 2017, 355: 18–22

13 Zhang L, Chen L, Zhou X, *et al.* Towards high-voltage aqueous metal-ion batteries beyond 1.5 V: The zinc/zinc hexacyanoferrate system. Adv Energy Mater, 2015, 5: 1400930

14 Hou Z, Zhang X, Li X, *et al.* Surfactant widens the electrochemical window of an aqueous electrolyte for better rechargeable aqueous sodium/zinc battery. J Mater Chem A, 2017, 5: 730–738

15 Lee B, Lee HR, Kim H, *et al.* Elucidating the intercalation mechanism of zinc ions into α-MnO_2 for rechargeable zinc batteries. Chem Commun, 2015, 51: 9265–9268

16 Xu C, Li B, Du H, *et al.* Energetic zinc ion chemistry: The rechargeable zinc ion battery. Angew Chem Int Ed, 2012, 51: 933–935

17 Zhang N, Cheng F, Liu J, *et al.* Rechargeable aqueous zinc-manganese dioxide batteries with high energy and power densities. Nat Commun, 2017, 8: 405

18 Huang J, Wang Z, Hou M, *et al.* Polyaniline-intercalated manganese dioxide nanolayers as a high-performance cathode material for an aqueous zinc-ion battery. Nat Commun, 2018, 9: 2906

19 Wang J, Wang JG, Liu H, *et al.* Zinc ion stabilized MnO_2 nanospheres for high capacity and long lifespan aqueous zinc-ion batteries. J Mater Chem A, 2019, 7: 13727–13735

20 Sun W, Wang F, Hou S, *et al.* Zn/MnO_2 battery chemistry with H^+ and Zn^{2+} coinsertion. J Am Chem Soc, 2017, 139: 9775–9778

21 Wang C, Zeng Y, Xiao X, *et al.* γ-MnO_2 nanorods/graphene composite as efficient cathode for advanced rechargeable aqueous zinc-ion battery. J Energy Chem, 2020, 43: 182–187

22 Guo C, Liu H, Li J, *et al.* Ultrathin δ-MnO_2 nanosheets as cathode for aqueous rechargeable zinc ion battery. Electrochim Acta, 2019, 304: 370–377

23 Alfaruqi MH, Mathew V, Gim J, *et al.* Electrochemically induced structural transformation in a γ-MnO_2 cathode of a high capacity zinc-ion battery system. Chem Mater, 2015, 27: 3609–3620

24 Zhang H, Liu Q, Wang J, *et al.* Boosting the Zn-ion storage capability of birnessite manganese oxide nanoflorets by La^{3+} intercalation. J Mater Chem A, 2019, 7: 22079–22083
25 Zhang N, Cheng F, Liu Y, *et al.* Cation-deficient spinel $ZnMn_2O_4$ cathode in $Zn(CF_3SO_3)_2$ electrolyte for rechargeable aqueous Zn-ion battery. J Am Chem Soc, 2016, 138: 12894–12901
26 Ao H, Zhao Y, Zhou J, *et al.* Rechargeable aqueous hybrid ion batteries: Developments and prospects. J Mater Chem A, 2019, 7: 18708–18734
27 Wu X, Li Y, Li C, *et al.* The electrochemical performance improvement of $LiMn_2O_4$/Zn based on zinc foil as the current collector and thiourea as an electrolyte additive. J Power Sources, 2015, 300: 453–459
28 Wang Y, Xia Y. A new concept hybrid electrochemical surpercapacitor: Carbon/$LiMn_2O_4$ aqueous system. Electrochem Commun, 2005, 7: 1138–1142
29 Tao H, Tong X, Gan L, *et al.* Effect of adding various carbon additives to porous zinc anode in rechargeable hybrid aqueous battery. J Alloys Compd, 2016, 658: 119–124
30 Wang F, Borodin O, Gao T, *et al.* Highly reversible zinc metal anode for aqueous batteries. Nat Mater, 2018, 17: 543–549
31 Yan J, Wang J, Liu H, *et al.* Rechargeable hybrid aqueous batteries. J Power Sources, 2012, 216: 222–226
32 Zhao J, Zhang J, Yang W, *et al.* "Water-in-deep eutectic solvent" electrolytes enable zinc metal anodes for rechargeable aqueous batteries. Nano Energy, 2019, 57: 625–634
33 Parker JF, Chervin CN, Pala IR, *et al.* Rechargeable nickel-3D zinc batteries: An energy-dense, safer alternative to lithium-ion. Science, 2017, 356: 415–418
34 Wan F, Zhang L, Dai X, *et al.* Aqueous rechargeable zinc/sodium vanadate batteries with enhanced performance from simultaneous insertion of dual carriers. Nat Commun, 2018, 9: 1656
35 Zhou W, Zhu D, He J, *et al.* A scalable top-down strategy toward practical metrics of Ni-Zn aqueous batteries with total energy densities of 165 W h kg^{-1} and 506 W h L^{-1}. Energy Environ Sci, 2020, 13: 4157–4167

Acknowledgements This work was supported by the National Key Research and Development Program of China (2016YFB0901503), Jiangsu Province Natural Science Research of Universities (19KJB150025), the National Natural Science Foundation of China (21875238 and 21831006), and Jiangsu Province Innovative and Entrepreneurial Doctor Project (KYQ19021 and KYQ19019).

Author contributions Zhang X, Dong M and Xiong Y synthesized the samples; Ao H and Liu M contributed to the analyses. Ao H and Hou Z wrote the paper. All authors contributed to the general discussion. Zhu Y and Qian Y checked the paper, corrected errors in the text, and polished the article to improve the quality of the article.

Conflict of interest The authors declare that they have no conflict of interest.

Supplementary Materials Experimental details and supporting data are available in the online version of the paper.

Zhiguo Hou is an associate professor at Jiangsu University of Technology. He received his BSc degree in 2013 from Jilin University. He received his PhD degree under the supervision of Prof. Yitai Qian at the University of Science and Technology of China. His research focuses on rechargeable aqueous metal ion batteries for energy storage.

Yitai Qian received his BSc degree in 1962 in chemistry from Shandong University. He was elected as an academician of Chinese Academy of Sciences in 1997. He is presently a full professor of the University of Science and Technology of China. In 2008, he became a fellow of the RSC. Professor Qian, as corresponding author, has published more than 800 peer-reviewed papers in journals including *Science*, *J. Am. Chem. Soc.*, *Angew. Chem. Int. Ed.*, *Adv. Mater.* with citations by important international journals exceeding 20,000 times. He has active research programs in solid state chemistry and the synthesis of nanomaterials for energy storage.

一种具有高能量密度、长循环寿命的水基可充电锰酸锂/锌实用电池

侯之国[1*], 张雪倩[1], 董梦飞[1], 熊亚丽[1], 张子祥[1], 敖怀生[2], 刘梦珂[2], 朱永春[2], 钱逸泰[2*]

摘要 本文报道了一种达到实际使用规格的水基可充电锌离子大电池, 该电池以锰酸锂为正极材料、锌粉为负极材料, 电流10 A时其能量密度可达80 W h kg^{-1}, 成本低于0.4 RMB kg^{-1}. 该电池体系使用一种专门开发的石墨-尼龙复合集流体作为正极集流体, 该复合集流体具有耐腐蚀性强、重量轻、价格便宜的特点. 通过向电解液中添加尿素的方法有效地抑制了锌枝晶生长. 该电池在10 A电流下充放电400次, 容量保留率达到90%. 该电池可应用于电动自行车、混动汽车及其他储能领域.

